EurJIC
European Journal of Inorganic Chemistry

Minireview
doi.org/10.1002/ejic.202000564

Chemistry Europe
European Chemical Societies Publishing

Hydrogen Production | *Very Important Paper* |

VIP

Structure-Functional Analysis of Hydrogen Production Catalyzed by Molecular Cobalt Complexes with Pentadentate Ligands in Aqueous Solutions

Ping Wang,[a][‡] Guangchao Liang,[b,c][‡] Charles Edwin Webster,*[c] and Xuan Zhao*[a]

Abstract: Hydrogen production from sunlight and water represents one promising solution to resolve the environmental problems caused by the consumption of fossil fuels and to meet the increasing global energy demands. Catalysts based on transition metal complexes have been extensively studied for electro- and photocatalytic production of hydrogen. Among the reported catalysts, molecular cobalt complexes have received special attention for hydrogen production over the past years. In this review, the recent progresses for electro- and photocatalytic production of hydrogen in aqueous solutions catalyzed by Co complexes with pentadentate ligands, with an emphasis of those developed in our lab, are discussed. Mechanistic investigations as well as future directions for hydrogen production by Co complexes are also discussed.

1. Introduction

A continuous energy support, currently based mainly on fossil fuels, is critical to maintain our rising living standards and societal development for the future. The environmental issues resulting from the consumption of fossil fuel have driven scientists to search for alternative clean and renewable forms of energy to meet the future global energy demands. Compared to other forms of energy, solar energy is the cleanest and one of the most abundant energy sources. The energy from sunlight reaching the Earth in one hour is estimated to be sufficient to support all human activities for one year.[1] Although the use of solar cells to convert sunlight into electricity has been achieved in practical applications,[2] the splitting of water into hydrogen and oxygen under solar irradiation provides an alternative way to store solar energy as chemical fuel, a process similar to that in the natural photosynthesis.[3]

The splitting of water consists of two half reactions: the oxidation of water to oxygen, and the reduction of protons to hydrogen. In nature, there exists three types of hydrogenases that catalyze hydrogen evolution reaction (HER): [FeFe]-, [NiFe]- and [Fe]-hydrogenases (Figure 1).[4] [FeFe]-hydrogenases, which are in general more active in hydrogen production than the other two types of hydrogenases, catalyze the reduction of protons to hydrogen reversibly at high rates (9000 s^{-1}) with nearly no overpotentials.[5] Such unsurpassed activity of [FeFe]-hydrogenases relies on the uniqueness of the active site cofactor, known as the H-cluster, consisting of a cuboidal $[Fe_4S_4]$ cluster attached to three cysteine residues connected via a fourth cysteine residue to the diiron moiety. The diiron cluster is where the catalysis occurs and includes two irons [one in proximal (Fe_p) and the other one in distal (Fe_d) position relative to the cluster] connected by a bridging azapropanedithiolate (adt) group, and the irons are coordinated by carbonyl and cyanide ligands. CO and CN^- are strong π-acceptor ligands; and, therefore, they can stabilize the low oxidation states of Fe center by metal-to-ligand backbonding.[6] It has also been demonstrated that CN^- ligands play a role in adjusting the redox potential of the H-cluster by raising the electron density on the iron centers.[7] The stabilized Fe_d with an open coordination site is responsible for the high activity of the enzyme.[6b] Furthermore, the amine in the bridging adt group can easily mediate proton transfer without changing the active site geometry.[8] There are three redox states of H-cluster participating in the catalytic proton reduction cycle: the active "oxidized" state H_{ox} with $[Fe^{I}Fe^{II}]$ connected to $[Fe_4S_4]^{2+}$, the active "reduced" state H_{red} with $[Fe^{I}Fe^{I}]$ connected to $[Fe_4S_4]^{2+}$, and the active "super-reduced" state H_{sred} with $[Fe^{I}Fe^{I}]$ connected to $[Fe_4S_4]^{+}$.[9] Similar transitions could be observed in different [FeFe] hydrogenases with different potentials.[10] In the [FeFe] hydrogenase from Desulfovibrio desulfuricans (DdH) bacteria, the transition from H_{ox} to H_{red} happens at a midpoint potential around –400 mV and the following irreversible reduction from H_{red} to H_{sred} occurs at –540 mV at pH 8.[11] Apfel and co-workers reported a possible catalytic mechanism for hydrogen production catalyzed by [FeFe] hydrogenase.[6b] $H_{red'}$ was formed from H_{ox} through a

[a] *Dr. P. Wang, Prof. X. Zhao*
Department of Chemistry, The University of Memphis, Memphis, Tennessee 38152, USA
E-mail: xzhao1@memphis.edu
https://www.memphis.edu/chem/faculty-zhao/index.php
[b] *Dr. G. Liang*
Department of Chemistry, University of Michigan, Ann Arbor, Michigan 48109, USA
[c] *Dr. G. Liang, Prof. C. E. Webster*
Department of Chemistry, Mississippi State University, Mississippi State, Mississippi 39762, USA
E-mail: ewebster@chemistry.msstate.edu
http://webster.chemistry.msstate.edu/index.html
[‡] P. W. and G. L. contributed equally to this work.
ORCID(s) from the author(s) for this article is/are available on the WWW under https://doi.org/10.1002/ejic.202000564.

Minireview
doi.org/10.1002/ejic.202000564

proton coupled electron transfer (PCET) to the $[Fe_4S_4]^{2+}$ cluster. The subsequent PCET process leads to instant proton reduction and the formation of a highly reactive apical hydride, H_{hyd}, which can react with a proton to generate H_2 heterolytically. Upon H_2 release, the resulting $H_{ox}H$ state loses a "regulatory" proton to form H_{ox} for the next catalytic cycle. An alternative pathway involving the participation of H_{sred} is also possible in the catalytic cycle for H_2 evolution.[6b]

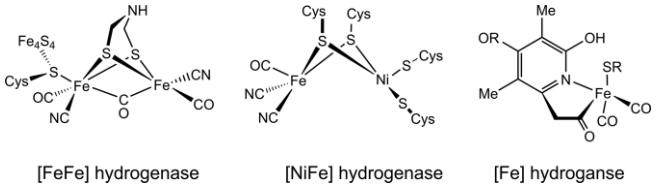

Figure 1. Active sites of the classic hydrogenase enzymes.

Inspired by natural hydrogenases, synthetic metal complexes, especially those based on earth abundant elements, have been developed to mimic the HER activity and to understand the mechanisms of catalytic HER by hydrogenases.[9,12] Catalysts based on metal–organic frameworks (MOFs)[13] and nanomaterials[14] have also been reported for hydrogen evolution. The advantages of molecular metal complexes in exploring the structure-function relationships and elucidating mechanistic details of HER have been demonstrated.[12g] Although Co is not found in the natural hydrogenases and it is less abundant on Earth than Fe or Ni,[15] molecular Co complexes have emerged over the past years for electro- and photocatalytic HER, especially in aqueous solutions.[12i,15–16]

2. Metrics for Evaluation of HER Catalysts

Ideally, an HER catalyst suitable for future practical applications should be easy to make, highly stable, active with low overpotentials in solutions over a wide range of pHs and temperatures, and no hazard to the environment. The electrocatalytic properties and activities of HER catalysts can be evaluated based on parameters such as the overpotential (η), Faradaic efficiency (FE), turnover number (TON), turnover frequency (TOF), and stability. Cyclic voltammetry (CV), square-wave voltammetry (SWV), linear sweep voltammetry (LSV) and bulk electrolysis (BE) are common techniques used to characterize the electrochemical properties of HER catalysts, including the redox potentials, overpotential, and Faradaic efficiency for HER.[17]

For a typical light driven HER, three components are generally required: a photosensitizer such as $[Ru(bpy)_3]^{2+}$ (PS1), $[Ir(ppy)_2bpy]^+$ (PS2), or $[Re(py)(bpy)(CO)_3]^+$ (PS3) for light absorption and electron transfer, a catalyst for water reduction, and a sacrificial reagent such as ascorbic acid (AA), triethyl-

Ping Wang received his B.S. in chemistry from Qingdao University in 2012, M.S. in organic chemistry from Zhengzhou University in 2015. He went to University of Memphis to pursue his degree under the supervision of Dr. Xuan Zhao since 2015 and he received his Ph.D. in May 2020.

Guangchao Liang is currently a research fellow in LSA Chemistry at the University of Michigan. He obtained his Ph.D. in Chemistry (2018) from Mississippi State University worked with Prof. Dr. Charles Edwin Webster. His research interests include computational chemistry, inorganic and organometallic chemistry, and catalysis and mechanism.

Charles Edwin Webster received his Ph.D. from the University of Florida (1999). He is Professor and Associate Department Head in the Department of Chemistry at Mississippi State University. He also serves on the Editorial Advisory Board of Organometallics. His research involves several areas of theoretical and computational chemistry, including areas of biological catalysis, bond activation, and structure and bonding.

Xuan Zhao obtained his B.S. from Nankai University (1993) and his Ph.D. at Texas A&M University (2002) under the direction of Professor Marcetta Y. Darensbourg. He was a postdoctoral fellow with Professor Yi Lu at University of Illinois at Urbana-Champaign from 2002 to 2008. He is currently Associate Professor in the Department of Chemistry at University of Memphis. His work is focused on inorganic, organometallic, bioinorganic chemistry and chemical biology, with particular interest in the design of metal complexes for hydrogen production.

amine (TEA), or triethanolamine (TEOA) serving as the electron donor. Mixed solvents such as CH_3CN/H_2O have also been used in photocatalytic HER due to the poor solubility of catalysts in water.[18] Higher activity and stability for proton reduction using quantum dots,[19] nanowire[20], or organic dyes as photosensitizers[21] have also been reported.

3. Hydrogen Production Catalyzed by Molecular Cobalt Complexes with Pentadentate Ligands from Other Groups

Due to their stability and solubility in aqueous solutions, molecular Co complexes with pentadentate ligands, with one site open for substrate binding and activation, have been developed over the past decade for electro- and photocatalytic hydrogen evolution. A series of Co complexes with pentadentate ligands reported by different research groups are presented in Figure 2. Their redox potentials, electrocatalytic activities, and photocatalytic properties for hydrogen production are summarized in Table 1, Table 2, and Table 3, respectively. The related discussions are introduced in the following sections.

3.1. Co Complexes with Pentapyridine and Pyridine-Pyrazine Ligands

In 2011, Chang, Long, and co-workers reported a Co polypyridyl complex **1a** for electrocatalytic hydrogen production in aqueous solution.[22] Complex **1a** displays a $Co^{II/I}$ peak at –1.00 V (vs. SHE) and another peak at –1.21 V (vs. SHE) after the formation of Co^{I} species in pH 7 phosphate buffer. Bulk electrolysis at –1.30 V (vs. SHE) for 60 h in a pH 7 phosphate buffer generated H_2 with a TON of 55,000 and 100 % FE. The introduction of electron withdrawing group $–CF_3$ (**1b**) led to a 0.16 V anodic shift to –0.84 V for the $Co^{II/I}$ redox potential and a 0.22 V decrease in overpotential for HER (**1a**: 0.62 V, **1b**: 0.40 V), while the introduction of $–NMe_2$ (**1c**) resulted in a 0.12 V cathodic shift to –1.12 V for the $Co^{II/I}$ redox potential. Among **1a**–**1c**, **1b** demonstrates the highest photocatalytic water reduction activity with a TON of 300 in the presence of PS1 and AA in 1.0 M phosphate buffer at pH 6. The improved HER activity under both electrocatalytic and photocatalytic conditions by **1b** demonstrates the electronic tuning of ligand scaffold as an effective approach to adjust the water reduction activity.[20]

Complexes **2a** and **2b** were reported in 2013 by Chang, Castellano, Long, and co-workers to investigate the effects of redox-active bpy ligands on electrocatalytic and photocatalytic proton reduction.[23] In comparison to **1a**, both **2a** and **2b** showed more positive redox potentials for the $Co^{II/I}$ event, suggesting the stabilization of low valent Co^{I} species. Similar to that of **1a** and **1b**, the introduced $–CF_3$ (**2b**) caused a 0.061 V positive shift for the $Co^{II/I}$ event with lower current density than that of **2a**. Compared to **2a**, the decreased electrocatalytic HER activity of **2b** probably results from the reduced π backbonding between Co^{I} and π* orbitals.[23] At pH 4 in the presence of PS1 and AA, TONs for photocatalytic H_2 evolution with **2a** and **2b** for 13 h were 1630 and 1390, respectively. The quantum yield values were determined as 3.6 % and 2.7 % for **2a** and **2b**, respectively.

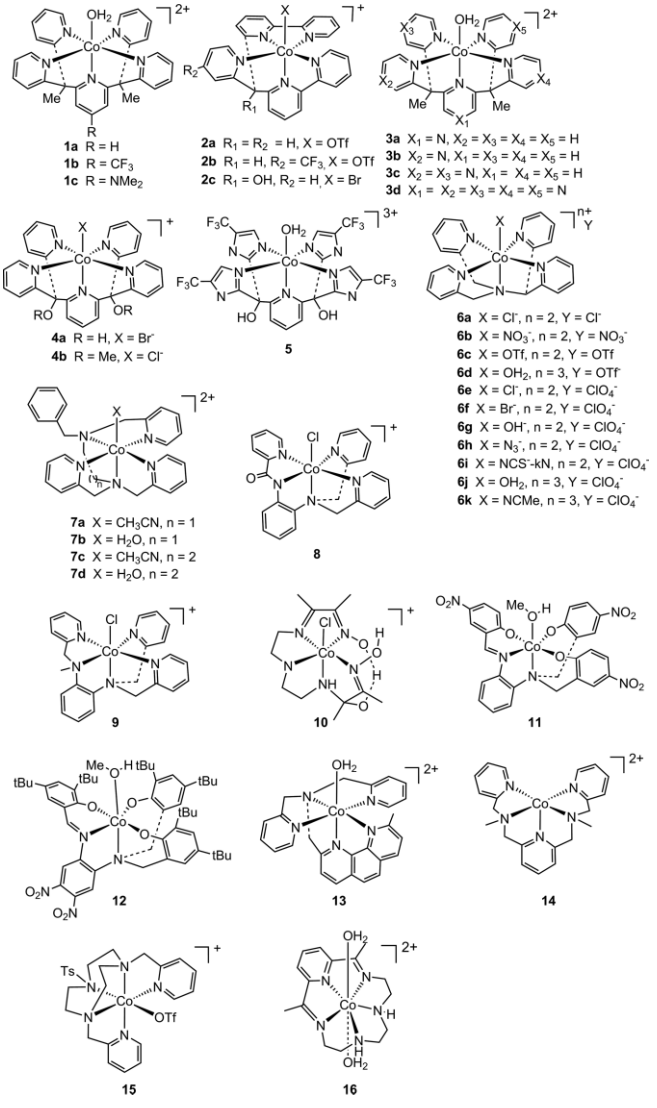

Figure 2. Reported Co complexes with pentadentate ligands from other groups.

Compared to pyridine, pyrazine has lower-energy π* orbitals which may enhance the formation of the metal-to-ligand backbonding and an easily reduced metal center for proton reduction. A series of Co complexes (**3a**–**3d**) with redox-active pyrazines were investigated for electrocatalytic hydrogen production in 2015 by Chang and co-workers.[24] In comparison to the $Co^{II/I}$ potential of **1a** in CH_3CN, the anodic shifts of 0.25, 0.17, 0.29, and 0.57 V were observed for **3a**–**3d**, respectively. Electrocatalytic hydrogen production from chloroacetic acid in acetonitrile solution showed that **3b** is the most active one by a factor of ca. 2 among **3a**–**3c** and the FEs of **3a**–**3c** were over 90 %. Bulk electrolysis at –1.2 V vs. SHE in neutral phosphate buffer demonstrated that **3c** is the most active catalyst with 350 coulombs of electrons passed for 12 h while 300 coulombs of electrons accounted for **3b** under same conditions. Photocatalytic water reduction at pH 5.5 in the presence of PS1 and AA demonstrated that **3b** is the most active one with over 2-fold enhancement than **3a** and **3c**, with TONs of 190 for **3a**, 450 for **3b**, and 170 for **3c**, even though **3c** is faster than **3a** and **3b** in

Table 1. Experimental redox potentials of complexes **1**–**16**.[a]

Cat.	Electrolyte	$Co^{III/II}$	$Co^{II/I}$	$Co^{I/0}$ or Ligand-based	Ref.
1a	CH_3CN (0.1 M nBu_4NPF_6)	0.24 V vs. Fc^+/Fc	–1.47 V vs. Fc^+/Fc	–2.36 V vs. Fc^+/Fc	[22]
1a	2 M phosphate buffer, pH 7	_	–1.00 V vs. SHE	–1.21 V vs. SHE	[22]
1b	CH_3CN (0.1 M nBu_4NPF_6)	0.34 V vs. Fc^+/Fc	–1.28 V vs. Fc^+/Fc	–2.21 V vs. Fc^+/Fc	[20]
1b	2 M phosphate buffer, pH 7	_	–0.84 V vs. SHE	_	[20]
1c	2 M phosphate buffer, pH 7	_	–1.12 V vs. SHE	_	[20]
2a	CH_3CN (0.1 M nBu_4NPF_6)	0.235 V vs. Fc^+/Fc	–1.2 V vs. Fc^+/Fc	–1.786 and –1.94 V vs. Fc^+/Fc	[23]
2b	CH_3CN (0.1 M nBu_4NPF_6)	0.31 V[c] vs. Fc^+/Fc	–1.14 V[c] vs. Fc^+/Fc	–1.706 and –1.86 V[c] vs. Fc^+/Fc	[23]
2c	0.1 M $NaBF_4$	_	–0.67 V[b] vs. SHE	_	[26]
3a	CH_3CN (0.1 M nBu_4NPF_6)	0.32 V vs. Fc^+/Fc	–1.22 V vs. Fc^+/Fc	–1.40 V vs. Fc^+/Fc	[24a]
3a	1 M phosphate buffer, pH 7	0.34 V vs. SHE	–0.68 V[e] vs. SHE	–0.76 V[e] vs. SHE	[24a]
3b	CH_3CN (0.1 M nBu_4NPF_6)	0.27 V vs. Fc^+/Fc	–1.30 V vs. Fc^+/Fc	–1.42 and –2.04 V vs. Fc^+/Fc	[24a]
3b	1 M phosphate buffer, pH 7	0.35 V vs. SHE	_	_	[24a]
3c	CH_3CN (0.1 M nBu_4NPF_6)	0.35 V vs. Fc^+/Fc	–1.18 V vs. Fc^+/Fc	–1.25 and –1.95 V vs. Fc^+/Fc	[24a]
3c	1 M phosphate buffer, pH 7	0.42 V vs. SHE	_	_	[24a]
3d	CH_3CN (0.1 M nBu_4NPF_6)	0.55 V vs. Fc^+/Fc	–0.90 V vs. Fc^+/Fc	–1.76 V vs. Fc^+/Fc	[24b]
4a	0.1 M $NaBF_4$	_	–1.1 V[b] vs. SHE	_	[26]
4b	CH_3CN (0.1 M $LiClO_4$)	0.09 V[c] vs. Fc^+/Fc	–1.71 V[c] vs. Fc^+/Fc	_	[27]
5	CH_3CN (0.1 M KNO_3)	–0.30 V[e] vs. Fc^+/Fc	–0.62 V[e] vs. Fc^+/Fc	–1.92 V[e] vs. Fc^+/Fc	[28]
6a	CH_3CN (0.1 M nBu_4NPF_6)	–0.26 V[c] vs. Fc^+/Fc	–1.86 V[c] vs. Fc^+/Fc	_	[29]
6b	CH_3CN (0.1 M nBu_4NPF_6)	–0.45 V[c] vs. Fc^+/Fc	–1.65 V[c] vs. Fc^+/Fc	_	[29]
6c	CH_3CN (0.1 M nBu_4NPF_6)	–0.43 V[c] vs. Fc^+/Fc	–1.63 V[c] vs. Fc^+/Fc	_	[29]
6d	CH_3CN (0.1 M nBu_4NPF_6)	–0.30 V[c] vs. Fc^+/Fc	–1.84 V[c] vs. Fc^+/Fc	_	[29]
6e	CH_3CN (0.1 M nBu_4NClO_4)	–0.28 V[d] vs. Fc^+/Fc	–1.79 V[d] vs. Fc^+/Fc	_	[30]
6f	CH_3CN (0.1 M nBu_4NclO_4)	–0.19 V[d] vs. Fc^+/Fc	–1.72 V[d] vs. Fc^+/Fc	_	[30]
6g	CH_3CN (0.1 M nBu_4NclO_4)	–0.86 V[e] vs. Fc^+/Fc	_	_	[30]
6h	CH_3CN (0.1 M nBu_4NclO_4)	–0.43 V[d] vs. Fc^+/Fc	–1.80 V[d] vs. Fc^+/Fc	_	[30]
6i	CH_3CN (0.1 M nBu_4NclO_4)	–0.29 V[d] vs. Fc^+/Fc	–1.70 V[d] vs. Fc^+/Fc	_	[30]
6j	CH_3CN (0.1 M nBu_4NclO_4)	–0.13 V[d] vs. Fc^+/Fc	–1.59 V[d] vs. Fc^+/Fc	_	[30]
6k	CH_3CN (0.1 M nBu_4NclO_4)	–0.14 V[d] vs. Fc^+/Fc	–1.58 V[d] vs. Fc^+/Fc	_	[30]
7a	THF (0.1 M nBu_4NPF_6)	–0.01 V vs. Fc^+/Fc	–1.69 V vs. Fc^+/Fc	–2.25 V vs. Fc^+/Fc	[31]
7b	THF (0.1 M nBu_4NPF_6)	_	–1.78 V vs. Fc^+/Fc	_	[31]
7b	1 M phosphate buffer, pH 7	_	–1.22 V vs. SHE	–1.40 V vs. SHE	[31]
7c	THF (0.1 M nBu_4NPF_6)	_	–1.66 V vs. Fc^+/Fc	_	[31]
7d	THF (0.1 M nBu_4NPF_6)	_	–1.80 V vs. Fc^+/Fc	_	[31]
8	CH_3CN (0.1 M nBu_4NPF_6)	–0.69 V vs. Fc^+/Fc	–1.99 V vs. Fc^+/Fc	–2.41 V vs. Fc^+/Fc	[32]
9	CH_3CN (0.1 M nBu_4NPF_6)	–0.02 V vs. Fc^+/Fc	–1.92 V vs. Fc^+/Fc	–2.39 V vs. Fc^+/Fc	[32]
10	CH_3CN (0.1 M nBu_4NPF_6)	–0.75 V vs. Fc^+/Fc	–1.68 V vs. Fc^+/Fc	–1.86 V vs. Fc^+/Fc	[33]
11	CH_3CN (0.1 M nBu_4NPF_6)	–0.57 V[e] vs. Fc^+/Fc	_	_	[34]
12	CH_3CN (0.1 M nBu_4NPF_6)	–0.44 V vs. Fc^+/Fc	_	_	[34]
13	CH_3CN (0.1 M nBu_4NPF_6)	–0.02 V vs. Fc^+/Fc	–1.43 V vs. Fc^+/Fc	–2.22 V vs. Fc^+/Fc	[35a]
14	CH_3CN (0.1 M nBu_4NPF_6)	_	–1.60 V vs. Fc+/Fc	–1.96 V vs. Fc+/Fc	[35b]
15	CH_3CN (0.1 M nBu_4NPF_6)	0.32 V[c] vs. Fc^+/Fc	–1.50 V[c] vs. Fc^+/Fc	–1.89 V[c] vs. Fc^+/Fc	[36]
15	H_2O (0.1 M KNO_3)	_	–1.05 V[c] vs. SHE	_	[36]
16	CH_3CN (0.1 M nBu_4NClO_4)		–1.32 V[e] vs. SHE	–1.87 V[e] vs. SHE	[38]

[a] $E(Fc^+/Fc)$ = 0.64 V vs. SHE. [b] From differential pulse polarography, converted from E(Ag/AgCl) = 0.20 V vs. SHE. [c] Converted from E(SCE) = 0.24 V vs. SHE. [d] Converted from $E(Ag/AgNO_3$ (0.01 M in $CH_3CN)) = 0.54$ V vs. SHE. [e] $E_{pc.}$

the beginning. Furthermore, the quantum yields for photocatalytic HER were determined as 0.26 ± 0.08 % for **3a**, 0.49 ± 0.02 % for **3b**, and 0.10 ± 0.06 % for **3c**. In summary, **3b** is the best catalyst among **3a**–**3c** due to its higher activity and stability while the overall lower stability and the anation of Co center accounts for the lower activity of **3c** for photocatalytic hydrogen production.

The research efforts from Chang and co-workers have demonstrated that the electro- and photocatalytic HER activity of Co complexes can be tuned through ligand modifications by changing electronic property, denticity, and/or incorporating redox-active motif.[12g,12h,20,22–23,25]

To compare the HER activities of two different pentadentate ligand scaffolds, complexes **2c** and **4a** were reported by Alberto and co-workers in 2013. The $Co^{II/I}$ redox potentials were observed at –1.1 V and –0.67 V (vs. SHE) for **2c** and **4a**, respectively, which are consistent with those reported by Chang.[23,26] Photocatalytic hydrogen production with PS3 and AA in ascorbic buffer at pH 4.1 generated H_2 with TONs of 1180 for **4a** and 1380 for **2c**. The activity difference between **2c** and **4a** was suggested to originate from their different geometrical properties: the distorted octahedral structure of **2c** resulted in less stable complex and increased activity, while **4a** with a stable and nearly an ideal octahedral geometry showed less activity.

In 2014, Natali, Lengo, Scandola, and co-workers reported another Co complex **4b**, and the CV of **4b** showed a catalytic proton reduction wave upon addition of trifluoroacetic acid (TFA).[27] The catalytic wave was observed before the $Co^{II/I}$ peak (–1.71 V vs. Fc^+/Fc), indicating the formation of Co^I is necessary for proton reduction catalyzed by the proposed Co^{III}–H interme-

Table 2. Bulk electrolysis of cobalt complexes **1–16** for electrocatalytic H_2 production.[a]

Cat.	Electrolyte	η [mV]	Potential (Proton source)	FE	[Current density (mA/cm^2)] / [Potential (V vs SHE)]	TON	TOF (mol H_2 (mol cat h)-1)	Ref.
1a	CH_3CN (0.1 M nBu_4NPF_6)	500	–1.10 V *vs* Fc^+/Fc (HOAc)	100 %	_	_	_	[22]
1a	2 M phosphate buffer, pH 7	660	–1.30 V *vs* SHE (H_2O)	100 %	1.5/(–1.00 V)	55,000 (60 h)	>920	[22]
1b	2 M phosphate buffer, pH 7	420	–0.96 V *vs* SHE (H_2O)	95 %	_	_	_	[20]
1b	0.1 M phosphate buffer, pH 7	_	_	_	0.16/(–0.89 V)	_	_	[20]
2a	CH_3CN (0.1 M nBu_4NPF_6)	530	_	90 %	_	_	_	[23]
2b	CH_3CN (0.1 M nBu_4NPF_6)	_	_	90 %	_	_	_	[23]
3a	CH_3CN (0.1 M nBu_4NPF_6)	_	–1.40 V *vs* Fc^+/Fc ($ClCH_2COOH$)	>90 %	_	_	_	[24a]
3a	1 M phosphate buffer, pH 7	ca. 500	–1.0 or –1.2 V *vs* SHE	ca. 100 %	1.1/(–1.2 V)	_	_	[24a]
3b	CH_3CN (0.1 M nBu_4NPF_6)	_	–1.40 V *vs* Fc^+/Fc ($ClCH_2COOH$)	>90 %	_	_	_	[24a]
3b	1 M phosphate buffer, pH 7	_	–1.0 or –1.2 V *vs* SHE	ca. 100 %	1.0/(–1.2 V)	_	_	[24a]
3c	CH_3CN (0.1 M nBu_4NPF_6)	_	–1.40 V *vs* Fc^+/Fc ($ClCH_2COOH$)	>90 %	_	_	_	[24a]
3c	1 M phosphate buffer, pH 7	_	–1.0 or –1.2 V *vs* SHE	ca. 100 %	0.91/(–1.2 V)	_	_	[24a]
3d	1 M phosphate buffer, pH 7	560	–1.3 V vs SHE	_	3.58/(–1.4 V)	_	0.14 s^{-1}	[24b]
5	phosphate Buffered MeCN/H_2O (1:1)	840	–1.42 V vs SHE	50 %	_	_	70 s^{-1}	[28]
7b	1 M phosphate buffer, pH 7	650	–1.25 V *vs* SHE	ca. 100 %	_	160,000 (60 h)	2,700	[31]
8	CH_3CN (0.1 M nBu_4NPF_6)	740	–2.14 V *vs* Fc^+/Fc (HOAc)	90 %	_	15.44 (3 h)	_	[32]
8	1 M phosphate buffer, pH 7	550	–1.5 V *vs* SHE (H_2O)	95 %	_	7,000 (18 h)	_	[32]
9	CH_3CN (0.1 M nBu_4NPF_6)	690	–2.14 V *vs* Fc^+/Fc (HOAc)	75 %	_	14.35 (3 h)	_	[32]
9	1 M phosphate buffer, pH 7	700	–1.5 V *vs* SHE (H_2O)	95 %	_	6,000 (18 h)	_	[32]
10	CH_3CN (0.1 M nBu_4NPF_6)	240	–2.14 V *vs* Fc^+/Fc (HOAc)	75 %	_	14.7 (3 h)	_	[33]
10	1 M phosphate buffer, pH 7	650	–1.5 V *vs* SHE (H_2O)	95 %	_	5,680 (17 h)	_	[33]
12	CH_3CN (0.1 M nBu_4NPF_6)	20	–2.11 V *vs* Fc^+/Fc (HOAc)	50 %	_	2.4 (3 h)	_	[34]
14	CH_3CN (0.1 M nBu_4NPF_6)	480	_	_	_	_	_	[35a]
15	CH_3CN (0.1 M nBu_4NPF_6)	590	_	_	_	_	3,420	[36]
16	0.1 M Phosphate buffer, pH 7	680	–1.1 V *vs* SHE	99 ± 4 %	3.3/(–1.1 V)	390 (1 h)		[37]

[a] η: overpotential; Potential: applied potential (V vs. SHE); FE: Faradaic efficiency.

diate. Photoinduced hydrogen production in the presence of 50 μM **4b**, PS1, and AA at pH 4 was examined with a TON of 187.[27] Like most other reported Co catalysts, the hydrogen production activity of **4b** is mainly limited by the partial decomposition of photosensitizer and catalyst.

By replacing equatorial pyridine with imidazole, Siewert and co-workers recently presented the electrocatalytic hydrogen production activity catalyzed by complex **5** in neutral or acidic solvent mixtures.[28] An onset potential of –1.28 V vs. NHE with 50 % FE and a catalytic rate constant of 70 s^{-1} at –1.42 V were determined for complex **5** in phosphate buffered MeCN/H_2O (1:1).

3.2. Co Complexes with Aminopyridine Ligands

To investigate the effects of monodentate ligands on the overall HER activities of Co complexes, the Wang and Blackman groups reported complexes **6a**–**6d** and **6e**–**6k** in 2014 and 2016, respectively, and both groups showed that the coordination of different monodentate ligands led to different redox potentials for the $Co^{III/II}$ and $Co^{II/I}$ peaks. Photocatalytic H_2 production activity in aqueous solutions at pH 4 by **6a**–**6d** with PS1 and AA were highly affected by the coordination of monodentate ligands according to Wang's results.[29] The most active one was **6a** with a TON of 15 (calculated based on 0.165 mL H_2 gener-

Table 3. Photocatalytic H_2 production by complexes **1–16**.

Cat.	Solvent	[Cat]	pH	Light	Irr. Time [h]	Amount of H_2	TON (mol H_2 (mol cat)$^{-1}$)	TOF (mol H_2 (mol cat h)$^{-1}$)	Ref.
1a	1 M phosphate buffer	50 mM	7	≥ 455 nm	8	0.42 mL	_	_	[20]
1a	1 M phosphate buffer	20 mM	6	520 nm	13	_	290	22	[20]
1b	1 M phosphate buffer	50 mM	7	≥ 455 nm	8	0.50 mL	_	_	[20]
1b	1 M phosphate buffer	20 mM	6	520 nm	13	_	300	23	[20]
1c	1 M phosphate buffer	50 mM	7	≥ 455 nm	8	0.25 mL	_	_	[20]
2a	H_2O	20 mM	4	520 nm	13	_	1,630	125	[23]
2b	H_2O	20 mM	4.5	520 nm	13	_	1,390	106	[23]
2c	H_2O	5 mM	4.1	LED 385 nm	15	69 mmol	1,380	920	[26]
2c	H_2O	0.1 mM	4.1	LED 385 nm	_	_	10,800	_	[26]
2c	H_2O	1 mM	5	LED 470 nm	11	290 mmol	33,300	5,900	[39]
2c	H_2O	100 mM	5	LED 470 nm	35	970 mmol	1,080	70	[39]
3a	H_2O	20 mM	5.5	452 nm	8	40 mmol	190	_	[24a]
3b	H_2O	20 mM	5.5	452 nm	8	90 mmol	450	_	[24a]
3c	H_2O	20 mM	5.5	452 nm	8	40 mmol	170	_	[24a]
4a	H_2O	5 mM	4.1	LED 385 nm	40	59 mmol	1,180	_	[26]
4b	1 M acetate buffer	50 mM	4	> 400 nm	1	45 mmol	187	486	[27]
6a	H_2O	50 mM	4	400–700 nm	3	0.165 mL	_	_	[29]
6b	H_2O	50 mM	4	400–700 nm	3	0.0305 mL	_	_	[29]
6c	H_2O	50 mM	4	400–700 nm	3	0.114 mL	_	_	[29]
6d	H_2O	50 mM	4	400–700 nm	3	0.123 mL	_	_	[29]
6e	H_2O	100 mM	4	400–700 nm	4	0.725 mL	59	_	[30]
6f	H_2O	100 mM	4	400–700 nm	4	0.769 mL	63	_	[30]
6h	H_2O	100 mM	4	400–700 nm	4	0.853 mL	70	_	[30]
6i	H_2O	100 mM	4	400–700 nm	4	0.834 mL	68	_	[30]
6j	H_2O	100 mM	4	400–700 nm	4	0.717 mL	59	_	[30]
6k	H_2O	100 mM	4	400–700 nm	4	0.753 mL	61	_	[30]
13	CH_3CN/H_2O (1:3)	100 mM	10	> 400 nm	4	105 mmol	210	_	[35a]
14	$CH_3CN/H2O$ (1:1)	0.1 mM	10	> 400 nm	4	145 μmol	290	_	[35b]
15	CH_3CN/H_2O (3:7)	50 mM	11.9	LED 447 nm	1.5	3.2 mL	690	_	[36]
16	1.1 M acetate buffer	1 μM	4.5	400–700 nm	22	_	1,660	5,400	[38]

ated by 50 μM **6a** in 10 mL buffer), while **6b** was least active with a TON of 3 (calculated based on 0.0305 mL H_2 generated by 50 μM **6b** in 10 mL buffer) under the same conditions. However, results from Crowley, Collomb, Blackman, and co-workers on Co complexes **6e**–**6k** demonstrated that there is little difference, with all complexes displaying TONs in the range of 60–70, for photocatalytic H_2 production in the presence of PS1 and AA.[30]

In 2013, Wang, Gloaguen, Sun, and co-workers reported new Co complexes **7a**–**7d** containing a tripyridine–diamine type pentadentate ligand for electrocatalytic proton reduction in neutral solution.[31] The $Co^{II/I}$ redox potential and the ligand-based couple for **7b** in pH 7 phosphate buffer were calculated to be –1.20 and –1.40 V vs. SHE, respectively. The overpotential for **7b** was determined as 0.65 V and bulk electrolysis by **7b** at –1.25 V (vs. SHE) for 60 h afforded hydrogen production with a TON of 160,000 and a Faradaic efficiency of 100 %, demonstrating **7b** serves as an efficient and stable electrocatalyst for proton reduction in neutral water.

Verani and co-workers reported in 2015 another two complexes **8** and **9** with different types of tripyridine–diamine ligands for electrocatalytic proton reduction.[32] The catalytic current enhancements were observed for both complexes at potentials near the $Co^{II/I}$ peak (**8**: –1.99 V; **9**: –1.92 V vs. Fc^+/Fc) upon addition of acetic acid, suggesting the electrocatalytic H_2 production. Under the same conditions, complex **8** displays a higher rate of proton reduction (7.39 s^{-1}) and higher TON (7,000) compared to those of **9** (4.29 s^{-1}, 6,000) by bulk electrolysis for 18 h in pH 7 phosphate buffer.

Complex **10**, reported by Verani and co-workers in 2015, catalyzed proton reduction with an overpotential of 0.65 V, achieving TONs of 950 over 3 h, and 5,680 over 18 h, at a current efficiency of 95 % by bulk electrolysis at –1.5 V (vs. SHE) in pH 7 phosphate buffer.[33] However, the UV/Vis and scanning electron microscopy (SEM) confirmed the generation of Co nanoparticles, which could catalyze hydrogen production.

Two Co complexes **11** and **12** with phenolate-based $[N_2O_3]$-type ligands were synthesized by Verani and co-workers in 2019, and there exists a significant difference of HER activities between **11** and **12** due to the distinct positions of the $–NO_2$ groups.[34] Complex **11** with nitro-substituted phenolates showed irreversible redox peaks and negligible HER activity, while complex **12** with functionalized phenylene moieties displayed reversible processes and HER activity at the very low overpotential of 0.02 V for HOAc. Based on these results, they concluded that the electronic nature and the structural position of a substituent would definitely affect the metal complexes' redox properties and catalytic activities.

Complexes **13** and **14** were reported by Chen and co-workers in 2015 and 2017, respectively, for electrocatalytic proton reduction in acetonitrile and photocatalytic proton reduction in CH_3CN/H_2O.[35] The redox potentials of $Co^{II/I}$ in CH_3CN for **13** and **14** are –1.43 and –1.60 V (vs. Fc^+/Fc), respectively. Addition of acetic acid to the catalysis solution triggered a current in-

Minireview
doi.org/10.1002/ejic.202000564

crease and a continued peak growth with more acid addition, indicating electrocatalytic HER by both **13** and **14**. Complex **13** displayed HER activity in the presence PS2 and TEA at pH 10 in CH_3CN/H_2O (1:3, v/v), with a TON of 210 under visible-light irradiation ($\lambda > 400$ nm).[35a] In CH_3CN/H_2O (1:1, v/v) mixed solvent at pH 10, photocatalytic proton reduction by complex **14** was achieved with a TON of 290 in the presence of PS2 and TEA.[35b] The decomposition of PS2 accounted for the cessation of H_2 evolution within the first 2 hours of photolysis for both complexes.

In 2014, Lloret-Fillol and co-workers reported another Co complex **15** with a macrocyclic pentadentate ligand for potential applications in both water reduction and water oxidation.[36] Electrocatalytic water reduction by **15** occurs at an overpotential of 590 mV, and the rate (k_e) and the TOF for HER were determined as 95 M^{-2} s^{-1} and 3,420 mol(H_2) mol(cat)$^{-1}$ h^{-1}, respectively. Complex **15** was also confirmed to be a stable catalyst due to the higher i_c/i_p ratio (60 at 60 mM trifluoroacetic acid) in water than that in CH_3CN (48 at 60 mM trifluoroacetic acid). Photocatalytic H_2 production by **15** was achieved with a TON of 690 using PS2 and TEA in CH_3CN/H_2O (3:7, v/v) mixed solvent, with 25 % activity in the presence of O_2. Dynamic light scattering (DLS) and nanoparticle tracking analysis indicated that nanoparticles did not contribute to the hydrogen production activity, while the formation of nanoparticles may contribute to the decomposition of catalyst during photocatalytic hydrogen production.

A distorted pentagonal bipyramid Co complex **16** with a nearly coplanar pentaaza-macrocyclic ligand was reported by Zhong, Lu, Sakai, and co-workers for electrocatalytic HER in 2019.[37] A quasi-reversible couple at $E_{1/2}$ = –0.80 V assigned for $[Co^{II}(L)(H_2O)_2]^{2+}/[Co^{II}(L^{\cdot-})(H_2O)]^{+}$ and an irreversible wave at –1.10 V (vs. NHE) for $[Co^{II}(L^{\cdot-})(H_2O)]^{+}/[Co^{0}(L)]$ were observed for complex **16** in a neutral aqueous 0.10 M $NaClO_4$ solution. A catalytic rate of 2210 s^{-1} was obtained for HER by **16**, and more importantly, complex **16** can retain 90 % of its activity under O_2 or CO. DFT computations suggested that the high tolerance of **16** to CO resulted from the labile character of the CO-bound species which could promote catalyst stability under CO during catalysis.

Thomas, Fortage, Collomb, and co-workers also studied the electrocatalytic and photocatalytic hydrogen production in water by complex **16**.[38] Photocatalytic HER in acetate buffer at pH 4.5 afforded a TON of 1660 at 1 μM **16**. The decoordination of an amine group possibly occurs at its Co^{I} form during catalytic HER.

4. Hydrogen Production by Molecular Cobalt Complexes with Pentadentate Ligands from Zhao's Lab

Inspired by the good solubility and stability of Co complexes with polypyridine ligands in aqueous solutions, a series of Co complexes active for electro- and photocatalytic hydrogen production have been synthesized and studied in Zhao's lab in collaboration with Webster, Schmehl, and Fujita for detailed computational and mechanistic studies of HER since 2012 (Figure 3).[40] Figure 4 shows the X-ray crystal structures of **17**, **19**, **20**, and **22**. The redox properties, electrocatalytic, and photocatalytic activities for HER were summarized in Table 4, Table 5, and Table 6, respectively.

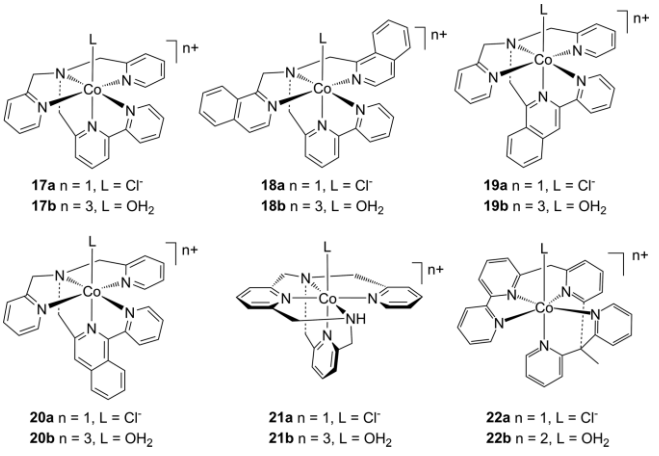

Figure 3. Co complexes with pentadentate ligands from Zhao's lab.

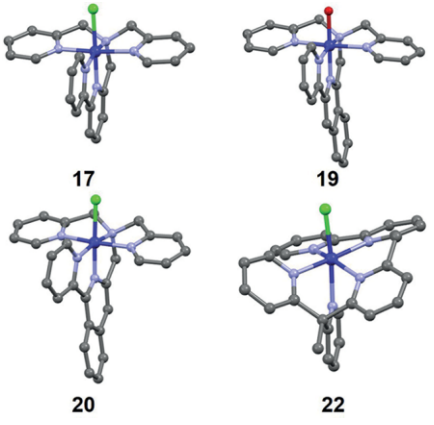

Figure 4. The X-ray structures of the cationic forms of **17**, **19**, **20**, and **22**.

Table 4. Experimental redox potentials (in V vs. SHE) of complexes **17b**–**22b** in 1.0 M pH 7.0 phosphate buffer.

Cat.	$(Co^{III/II})$[a]	$(Co^{II/I})$[b]	$(Co^{III}$-H/Co^{II}-H)[b]	Ref.
17b	0.15	–0.84	–0.96	[40a]
18b	0.14	–0.73	–0.82	[40b]
19b	0.11	–0.93	–1.04	[40c]
20b	0.12	–0.64	–0.78	[40c]
21b	0.10	–1.19	–1.26	[40d]
22b	–	–0.70	–1.14	[40e]

[a] Glassy carbon electrode. [b] Mercury drop electrode.

Table 5. Bulk electrolysis of cobalt complexes **17b–22b** for electrocatalytic H_2 production in pH 7.0 phosphate buffer.

Cat.	η[a]	Potential	FE[%]	[cat]	TON(mol H_2 (mol cat)$^{-1}$)	Ref.
17b	600	–1.4	99 ± 1	50 μM	400 (1 h)	[40a]
		–1.3	98 ± 2	1 μM	54,200 (20 h)	
18b	530	–1.4	99 ± 1	50 μM	890 (1 h)	[40b]
19b	735	–1.4	98.2	50 μM	300 (1 h)	[40c]
20b	735	–1.4	90.3	50 μM	110 (1 h)	[40c]
21b	610	–1.4	96.7	50 μM	140 (1 h)	[40d]
22b	586	–1.3	97.5 ± 0.5	1 μM	266,300 (20 h)	[40e]

[a] η: overpotential (mV); Potential: applied potential (V vs. SHE); FE: Faradaic efficiency.

Table 6. Photocatalytic H_2 production by complexes **17b–22b** in the presence of 0.1 M AA and 0.5 mM PS1.

Cat.	Electrolyte	[Cat]	pH	TON	Ref.
17b	1 M acetate buffer	0.5 μM	4	4,400 (3 h)	[40a]
	1 M phosphate buffer	5 μM	7	390 (3 h)	
18b	1 M phosphate buffer	5 μM	7	830 (3 h)	[40b]
19b	1 M acetate buffer	0.5 μM	4	6,980 (3 h)	[40c]
20b	1 M acetate buffer	0.5 μM	4	220 (3 h)	[40c]
21b	1 M phosphate buffer	5 μM	7	100 (3 h)	[40d]
22b	1 M phosphate buffer	0.5 μM	7	15,000 (2 d)	[40e]

4.1. Co Complexes with Aminopyridine Ligands

The Co complexes **17a** and **17b** with the aminopyridine ligand, DPA-Bpy (DPA-Bpy = N,N-bis(2-pyridinylmethyl)-2,2′-bipyridine-6-methanamine), were reported by our group in 2012 for electro- and photocatalytic water reduction.[40a] While the DPA-Bpy ligand was initially designed for the oxidation of water by $[Ru(DPA\text{-}Bpy)(OH_2)]^{2+}$, the Co complexes of DPA-Bpy ligand, **17a** and **17b**, were synthesized and tested for their activities on the reduction of water to hydrogen.[22,41] In pH 7 phosphate buffer, complex **17b** displayed three redox couples at –0.15, –0.84, and –0.96 V (vs. SHE), assignable to the $Co^{III/II}$, $Co^{II/I}$, and Co^{III}–H/Co^{II}–H couples, respectively (Table 4). An overpotential of 600 mV for HER was determined for **17b** in pH 7 phosphate buffer. Electrocatalytic hydrogen production through bulk electrolysis at –1.4 V (vs. SHE) by **17b** at pH 7 was achieved with a FE of 99 % and a TOF of 1,400 L H_2 $(mol\ cat)^{-1}\ h^{-1}\ (cm^2\ Hg)^{-1}$. Under optimal conditions, light driven proton reduction was achieved with a TON over 4,400 and a TOF of 4,000 mol H_2 $(mol\ cat)^{-1}\ h^{-1}$ in the presence of 0.5 μM **17b**, 0.1 M AA, and 0.5 mM PS1 in 1 M acetate buffer at pH 4. The decomposition of both catalyst and photosensitizer occurred during the photocatalytic H_2 evolution, and the dissociation of Co metal from ligand scaffold may account for the catalyst deactivation.

To study the possible electronic effects of ligand scaffold on HER activity and to further improve the proton reduction activity of **17b**, new complexes **18a** and **18b** were synthesized by replacing the equatorial pyridyls with more basic isoquinoline groups.[40b] Electro- and photocatalytic H_2 production by **18b** indicated a significant activity improvement with a lower overpotential, and higher TON and TOF in neutral conditions possibly resulting from the more stable low-valent Co center. In pH 7 phosphate buffer, the $Co^{II/I}$ and Co^{III}–H/Co^{II}–H couples were observed at –0.73 V and –0.82 V (vs. SHE), respectively. The shift to more positive potentials of **18b** than those of **17b** could possibly result from the more stabilized low-valent Co center by the more conjugated isoquinoline groups. Compared to **17b**, the electrocatalytic HER by **18b** at pH 7 occurs at an overpotential of 530 mV (600 mV for **17b**) with TONs of 890 at an applied potential of –1.4 V vs. SHE (400 for **17b**) and 300 at –1.2 V vs. SHE (30 for **17b**). Besides, **18b** lasts for more than 5 h in the bulk electrolysis experiment while **17b** is only active for 3 h at an applied potential of –1.4 V vs. SHE. Complex **18b** exhibited the best activity at pH 5 for photocatalytic proton reduction, with a TON of 1,690 at 5 μM **18b**. In 1 M phosphate buffer at pH 7, **18b** displayed activity for photocatalytic H_2 production with a TON of 830 which is more than two times of that produced by **17b** (390) under the same conditions, demonstrating **18b** is more active than **17b** for photocatalytic water reduction in neutral aqueous solutions. The decomposition of catalysts **17b** and **18b** was also observed under the photolysis conditions.

Our studies of **17b** and **18b** motivated the design and syntheses of complexes **19** and **20** by replacing the axial pyridyl in **17b** with isoquinoline group to further explore the electronic and steric effects on HER.[40c] The experimental results indicated that there is significant activity difference between **19** and **20** even though there is a slight structural difference on the position of the isoquinoline moiety. The X-ray crystal structures confirmed a planar bpy unit in **19** and a nonplanar bpy unit in **20**. In pH 7 phosphate buffer, complexes **19b** displayed redox potentials at –0.93 V and –1.04 V, while **20b** showed redox events at –0.64 V and –0.78 V (vs. SHE), assignable to the $Co^{II/I}$ and Co^{III}–H/Co^{II}–H couples, respectively. Although there exist much different potentials between **19b** and **20b**, both complexes catalyze electrocatalytic HER at similar overpotentials, suggesting that there is no direct correlation between the redox potentials of Co centers and the overpotentials for electrocatalytic HER. A higher Faradaic efficiency of 98.2 % for **19b** was determined compared to that of 90.3 % for **20b**. Electrocatalytic HER occurs with TONs of 300 and 110 for **19b** and **20b**, respectively, after one-hour bulk electrolysis at –1.4 V vs. SHE in pH 7 phosphate buffer, demonstrating that **19b** is about 3 times as active as **20b** under the same conditions. For photocatalytic HER using PS1 as photosensitizer and AA as electron donor, complex **19b** showed the best activity at pH 4, while **20b** was the most active at pH 5. In pH 4 acetate buffer, **19b** (TON: 6,980) was about 32 times as active as complex **20b** (TON: 220) in photocatalytic HER. Furthermore, **19b** (TON: 220) was 7 times more active than **20b** (TON: 30) in neutral conditions for photocatalytic H_2 production. Therefore, the activities of both electro- and photocatalytic HER confirmed that **19b** with a planar bpy unit is much more active than **20b** with a distorted bpy unit. Besides, photocatalytic hydrogen production by complex **19b** also displayed better activity than **17b** under the same conditions. Our studies of complexes **17**–**20** suggest that a conjugated and planar bpy unit and its isoquinoline analogue may play a key role in controlling the redox and catalytic properties of cobalt complexes for HER. The conjugated bpy unit, as an important structural feature for HER, could possibly contribute to the stabilization of the low valent Co^{I} species through π-back bonding between Co and the bpy unit.[40c,42] While **17**–**20** display vastly different redox and catalytic properties for HER, all complexes exhibit similar stability (2–3 hours) under photocatalytic conditions since all Co complexes contain an analogous ligand scaffold derived from DPA-Bpy.

4.2. Co Complexes with a Macrocyclic Ligand

In 2019, we reported the synthesis of Co complexes **21a** and **21b** with a macrocyclic pentadentate ligand for proton reduction in aqueous solutions.[40d] The macrocyclic ligand of **21** was attempted as a cage to prevent the dissociation of Co ion under

catalysis conditions. However, complex **21b** exhibited much lower electro- and photocatalytic activities than **17b**, **18b**, and **19b**. In comparison to complexes **17**–**20**, **21b** displays the most negative redox potentials at –1.19 and –1.26 V vs. SHE for the $Co^{II/I}$ and Co^{III}–H/Co^{II}–H couples, respectively. Electrocatalytic proton reduction at –1.4 V (vs. SHE) in pH 7 phosphate buffer by **21b** only gave a TON of 140. Complex **21b** also displayed much lower activity for photocatalytic water reduction with a TON of 100 compared to **17b**, **18b**, and **19b** under neutral conditions. The best pH for photocatalytic water reduction by **21b** was found to be at pH 6 (TON: 200). In comparison to **17b**, the decreased HER activity of **21b** could possibly originate from the addition of one more amine group, which may be responsible for the decreased activity of **21b** for HER.

4.3. Co Complexes with a Pentapyridine Ligand

Our studies of complexes **17**–**20** suggested that the dissociation of the Co ion, possibly Co^{I} species, from the ligand scaffold is responsible for catalyst decomposition during H_2 production under catalysis conditions.[40a,40b] The tertiary amine group(s) in DPA-Bpy and the macrocyclic ligand of complex **21** could possibly contribute to the dissociation of the Co ion during catalysis. Co catalysts based on only pyridine ligands generally display higher stability, especially for photocatalytic HER, than those containing more tertiary amine groups. We expected that the replacement of the tertiary amine group in **17b** with a softer pyridine group may stabilize the low valent Co^{I} species during catalysis. Recently, we reported the synthesis, characterization, and activity studies of new Co complexes **22a** and **22b**.[40e] Complex **22b** shows the $Co^{II/I}$ and Co^{III}–H/Co^{II}–H redox events at –1.19 V and –1.26 V vs. SHE, respectively, in pH 7 phosphate buffer. Electrocatalytic HER by **22b** occurs at an overpotential of 586 mV. Bulk electrolysis at –1.3 V vs. SHE for 20 h in neutral aqueous solutions demonstrated that **22b** (TON: 266,300) is about 4 times more active than that of **13b** (TON: 54,200). Photocatalytic hydrogen production by complex **22b** was achieved with a TON of 15,000 in neutral conditions.[40e] Furthermore, complex **22b** exhibited the best activity at pH 7 and showed continuous H_2 production over 2 days, while complex **17b** only lasted for 3 hours with a TON of 450. Therefore, complex **22b** was 5 and 15 times as active as complex **17b** for electro- and photocatalytic H_2 production in neutral aqueous solution, respectively. With respect to **17b**, the substitution of amine with a softer pyridyl group, in combination with a conjugated bpy unit, does indeed improve the stability and activity of **22b** for both electro- and photocatalytic HER.

5. Mechanistic Studies for Hydrogen Production by Co Complexes with Pentadentate Ligands

5.1. Electrocatalytic Hydrogen Production

Both mononuclear and binuclear pathways have been proposed to account for H_2 evolution catalyzed by molecular Co complexes.[15,43] Scheme 1 shows one pathway for the aqueous hydrogen production catalyzed by cobalt complexes (Co^{III}–OH_2 species) via a modified electron transfer (E)–proton transfer (C)–electron transfer(E)–proton transfer (C) (mod-ECEC) followed by the heterolytic coupling of protonated Co^{II}–H species to generate the H_2 molecule.[12g,16c,44] In the modified ECEC pathway, Co^{III}–OH is first generated via the deprotonation of Co^{III}–OH_2, and a $1e^-/1H^+$ PCET process of Co^{III}–OH produces the Co^{II}···OH_2 species. The subsequent formation of Co^{I} and Co^{III}–H species has been suggested as critical intermediates involved in H_2 production.[45]

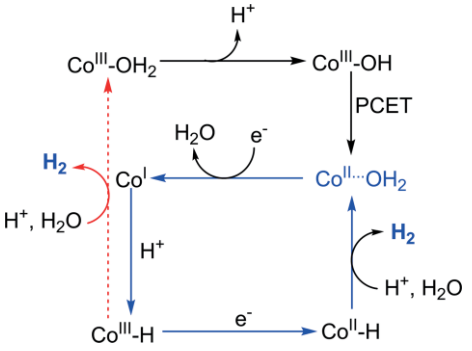

Scheme 1. Pathways of aqueous hydrogen production catalyzed by cobalt complex.

Formation of Co^{I} Intermediate

By employing transient pulse radiolysis, Fujita and co-workers examined the individual steps of proton reduction and characterized the key intermediate (Co^{I} and Co^{III}–H) species involved in H_2 production by complex **17b**.[40g] The formation of Co^{I} species of **17b** occurs at a rate constant of 7×10^9 M^{-1} s^{-1} upon the exposure of its Co^{II}–OH form to e_{aq}^- at pH 12.5.[40g] The absorption of Co^{I} species at 650 nm suggests the electron density is mainly localized on the Co center. DFT computations of **17b** and its derivatives suggested that a transient $[Co^{I}(\kappa^4\text{-L})(OH_2)]^+$ intermediate may also be involved in the formation of the penta-coordinated Co^{I} species.[40c,40g] It is worth noting that possible conversion between the square pyramidal triplet $^3Co^{I}$ and the trigonal bipyramidal singlet $^1Co^{I}$ species could exist in the aqueous hydrogen production catalyzed by cobalt complex **17b**.

Formation of Co-Hydride Intermediate

The structures of three Co^{III}–H species of $[Cp^X(t\text{BuP})_2(^{Ph}N)_2]$-$Co^{III}$-H](BF$_4$) (X = H, C_6F_5 and C_5F_4N), obtained by the direct protonation of the related Co^{I} species, have been reported and characterized by single-crystal X-ray crystallography.[46] The decay of the Co^{I} species of **17b** occurs at a rate of $(1.9 \pm 0.3) \times 10^4$ s^{-1} accompanied with the formation of the Co^{III}–H species which shows an absorption maximum at 370 nm. The pK_a of the Co^{III}–H species was calculated to be ≥14, consistent with the value of 13.9 predicted from the DFT computations. By utilizing nanosecond time-resolved infrared (TRIR) spectroscopy, a later study by Fujita's group allowed unambiguous assignment of the transient species as Co^{III}–H based on the isotopic shift of the ν(Co–H) stretching frequency (ν_H/ν_D = 1.4).[47]

The decay of the Co^{I} species of **17b** is independent of proton concentration from pH 3 to pH 12.5, suggesting that the protonation of Co^{I} is not a rate-determining step, and a rate determining reaction must occur before the formation of Co^{III}–H. The Co^{I} species of **17b** must undergo some structural change prior to accepting the proton, and this structural transformation represents the rate-determining step (RDS) in the overall formation of the Co^{III}–H intermediate. This RDS may originate from the slow removal of a solvent ligand in the intermediate and the significant inner- and outer-sphere reorganization energies predicted from DFT computations.[40g] A recent study by Luber, Llobet, Gimbert-Suriñach, and co-workers on the hydrogen production catalyzed by cobalt tetraazamacrocycle complexes $[Co(^{R}N_3Py)Cl_2]^{+}$ (R = H, CH_2OH. N_3Py = 2,12-dimethyl-3,7,11-triaza-1(2,6)-pyridinacyclododecaphane-2,11-diene) suggests that the formation of Co^{III}–H via the protonation of Co^{I} species is the rate-determining step in electrocatalytic hydrogen production.[48]

The formation of Co^{III}–H via the protonation of Co^{I} species as the rate-determining step was also presented in electrocatalytic hydrogen production catalyzed by the CH_3CN-bound form of **1a** in CH_3CN.[49] Furthermore, the Co^{III}–H intermediate of **17b** is stable at pH 12.5 for at least 5 s, suggesting that H_2 production is unlikely to occur via the reaction of two Co^{III}–H species in a bimolecular fashion. Therefore, from pulse radiolysis experiment, the kinetic formations of Co^{I} and Co^{III}–H intermediates have been characterized for electrocatalytic H_2 production by complex **17b**.[40g]

H_2 Evolution

DFT computations of HER by complexes **17**–**22** have suggested that the protonation of one equatorial pyridine in the Co^{II}–H species leads to the formation of the dissociated protonated pyridine Co^{II}–H (ligand-protonated Co^{II} hydride) species, and subsequent heterolytic coupling of the proton from the dissociated pyridine with the hydride forms the H–H bond and releases an H_2 molecule. Relatively high free energies of activation indicate no H–H bond could be formed via the unfavorable heterolytic coupling with the Co^{III}–H species (Scheme 1).

The H–H bond formation via the intramolecular proton-hydride heterolytic coupling in a ligand-protonated Co^{II} hydride has been suggested as the rate-determining step in the electrocatalytic H_2 evolution by $[Co(bapbpy)Cl]^{+}$ (bapbpy: 6,6′-bis(2-aminopyridyl)-2,2′-bipyridine) with HBF_4 used as the proton source, because the effect of the concentration of catalyst on the catalytic midwave potential and the effect of concentration of acid on catalytic current were not observed.[44]

5.2. Photocatalytic Hydrogen Production

During photocatalytic hydrogen production, the excited photosensitizer (PS*) can be quenched by two pathways (Scheme 2): oxidative quenching where the generated PS* from light absorption is oxidized by Co catalysts, and the reductive quenching where PS* is reduced by electron donor. Photocatalytic systems using PS1 as photosensitizer and AA as electron donor generally occur via the reductive quenching pathway. When AA

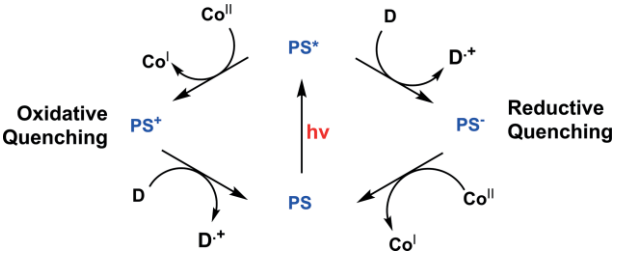

Scheme 2. Oxidative quenching (left) and reductive quenching (right) pathways for photocatalytic hydrogen production.

is used as electron donor, the oxidized product of AA, namely DHA (dehydroascorbic acid), can self-inhibit AA-driven photocatalysis by back electron transfer between $[Ru(bpy)_2(bpy^{\bullet-})]^{+}$ and DHA.[39] The addition of tris-(2-carboxyethyl)phosphine (TCEP) has been shown to improve overall photocatalytic HER activity by reducing DHA back to AA.[39,50]

Mechanistic studies for photocatalytic hydrogen production by **17b** were carried out by the groups of Schmehl and Fujita to characterize the key Co^{I} and Co^{III}–H intermediates for hydrogen production by flash photolysis spectroscopy.[40f] Upon light absorption, the excited state of PS1 was reductively quenched by AA with a rate constant of 1.0×10^{7} M^{-1} s^{-1} at pH 4, and the charge separation yield to generate the reduced $[Ru(bpy)_3]^{+}$ is 0.78. At pH 4, the rate constants for the reduction of the Co^{III} and Co^{II} species by $[Ru(bpy)_3]^{+}$ were determined to be 5×10^{9} M^{-1} s^{-1} and 4.9×10^{9} M^{-1} s^{-1}, respectively, near the diffusion limit with an approximate efficiency of over 90 % for the reduction of cobalt. The overall quantum yield for H_2 production was measured to be 0.07 at pH 4, suggesting an efficiency of 46 % for H_2 production from the reaction of Co^{I} species with water.[40f]

A photolysis study by Fujita and co-workers has also confirmed the formation of the Co^{I} and Co^{III}–H intermediates during photocatalytic H_2 production by complex **17b**.[40g] The decay of the photogenerated $[Ru(bpy)_3]^{+}$ species was accompanied with the formation of Co^{I} species, which decayed to another species with a weak absorbance at ca. 370 nm attributed to the Co^{III}–H intermediate. The apparent lifetime of the Co^{I} species was determined as 30 μs ($k = 3.3 \times 10^{4}$ s^{-1}), consistent with that from the pulse radiolysis study.

The Co^{I} intermediate of **17b** produced during aqueous photocatalytic HER was also characterized by X-ray transient absorption spectroscopy (XTA) and optical transient by Wu and co-workers in 2016.[42] Structural analysis from the X-ray absorption near-edge structure (XANES), and extended X-ray absorption fine structure (EXAFS), as well as DFT computations revealed the Co^{I} species as a penta-coordinated Co center with significant Co–N bond contraction of 0.09 ± 0.03 Å with respect to its Co^{II} analogue. Such bond contraction from Co^{II} to Co^{I} species suggested the stabilization of the Co^{I} intermediate due to the metal-to-ligand π backbonding.

Long, Chang, Castellano, and co-workers reported the detection of an active Co^{I} species of **2a** which displays a weak and broad absorption band between 450–700 nm during photocatalytic HER.[25b] Using time-resolved Co K-edge X-ray absorption spectroscopy, Smolentsev and co-workers reported the charac-

Minireview
doi.org/10.1002/ejic.202000564

terizations of the Co^{I} intermediate of catalyst **2c** during photocatalytic HER.[51] Upon reduction, the pyridine group in the hexa-coordinated high-spin Co^{II} form dissociates to yield the intermediate Co^{I} species as a tetracoordinated Co center with a square-planar geometry. The resulting pyridinium from the protonation of the dissociated pyridine group was proposed as an active intramolecular proton donor to facilitate the formation of Co–H intermediates and subsequent H–H bond formation.[51]

5.3. Deactivation of Catalyst

Besides the dissociation of the cobalt ion from the ligand scaffold, the decay of Co^{I} intermediate[42] and the formation of metallocycle by-products via ligand intramolecular metalation[40c,40e,52] were proposed as the possible reasons for the deactivation of cobalt catalysts during hydrogen production. The various protonation pathways for the Co^{I} species of **22b** are illustrated in Scheme 3. Instead of direct protonation of the Co^{I} metal ion to form the Co^{III}–H species, multiple other protonations could also occur in the penta-coordinated Co^{I} species. The more favorable protonation on the axial pyridine N^5 to form a metallocycle Co^{III} by-product (Co^{III}–N^5H, –8.0 kcal mol^{-1}, Scheme 3) compared to the formation of the Co^{III}–H species (–4.5 kcal mol^{-1}, Scheme 3) may explain the observed decreased activity of **22b** in photocatalytic H_2 production in low pH solutions.

The analogous favorable formation of a metallocycle Co^{III} species by-product upon the protonation of the Co^{I} species are also shown in other cobalt polypyridyl complexes, and the relative energetic differences between the favorable formation of the unreactive metallocycle complex compared to active Co^{III}–H intermediate could address the catalytic activities of the cobalt polypyridyl complexes. The relatively high Gibbs free energies of activation for the transfer between the protonated equatorial pyridine and Co^{III}–H species could also decrease the activity. The various pyridine ligand protonation and formation of metallocycle by-products finally lead to catalyst deactivation.

Another interesting finding that may also explain catalyst deactivation is the protonation of the Co^{II}–H species (Scheme 4). Once the Co^{II}–H species was formed by the electron transfer to the Co^{III}–H species, multiple protonations could also occur in the octahedral Co^{II}–H species. The H–H bond formation could be easily accomplished by the equatorial pyridine ligand-protonated Co^{II}–H species. The Gibbs free energies of activation for proton-hydride heterolytic coupling in Co^{II}–H–N^1H, Co^{II}–H–N^2H, and Co^{II}–H–N^4H are 10.9, 13.0, and 11.8 kcal mol^{-1}, respectively (Scheme 4).

The deactivation of the water reduction Co complex $[Co^{III}(L^1)(pyr)_2]PF_6$ ($(L^1)^{2-}$ = bis-amido pyridine ligand, pyr = pyrr-

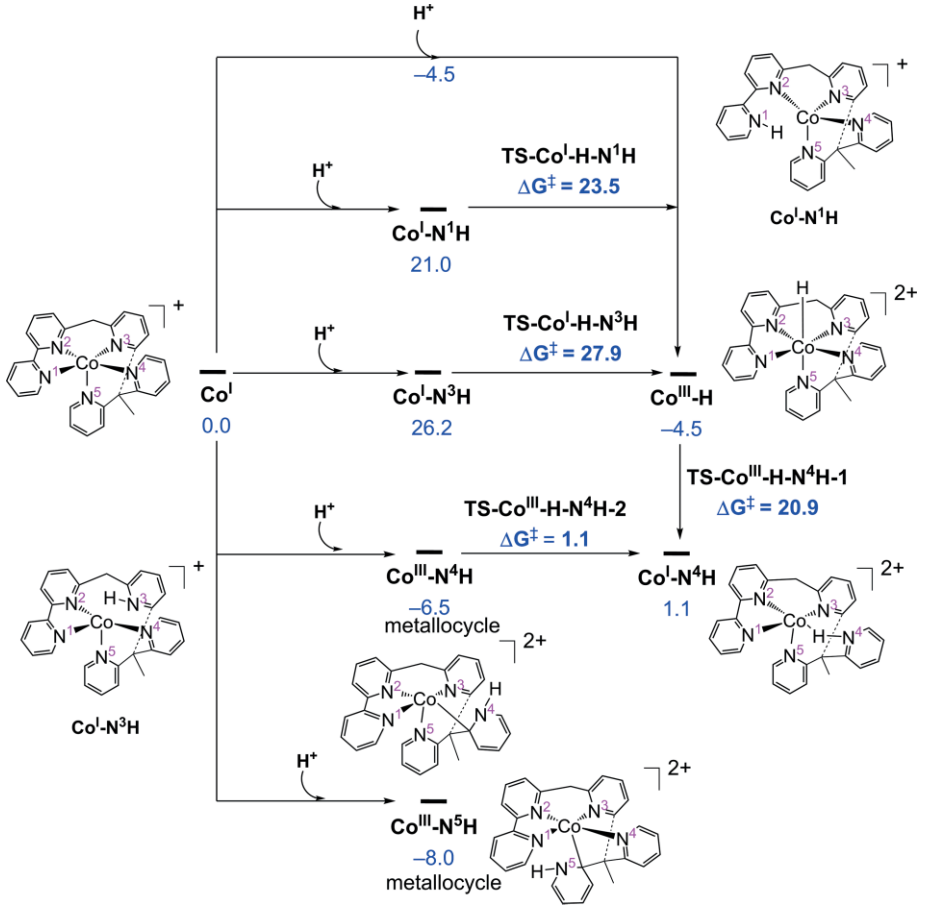

Scheme 3. Protonation pathways of singlet Co^{I} species. Energies are given in kcal/mol. Adapted from ref.[40e]

Minireview
doi.org/10.1002/ejic.202000564

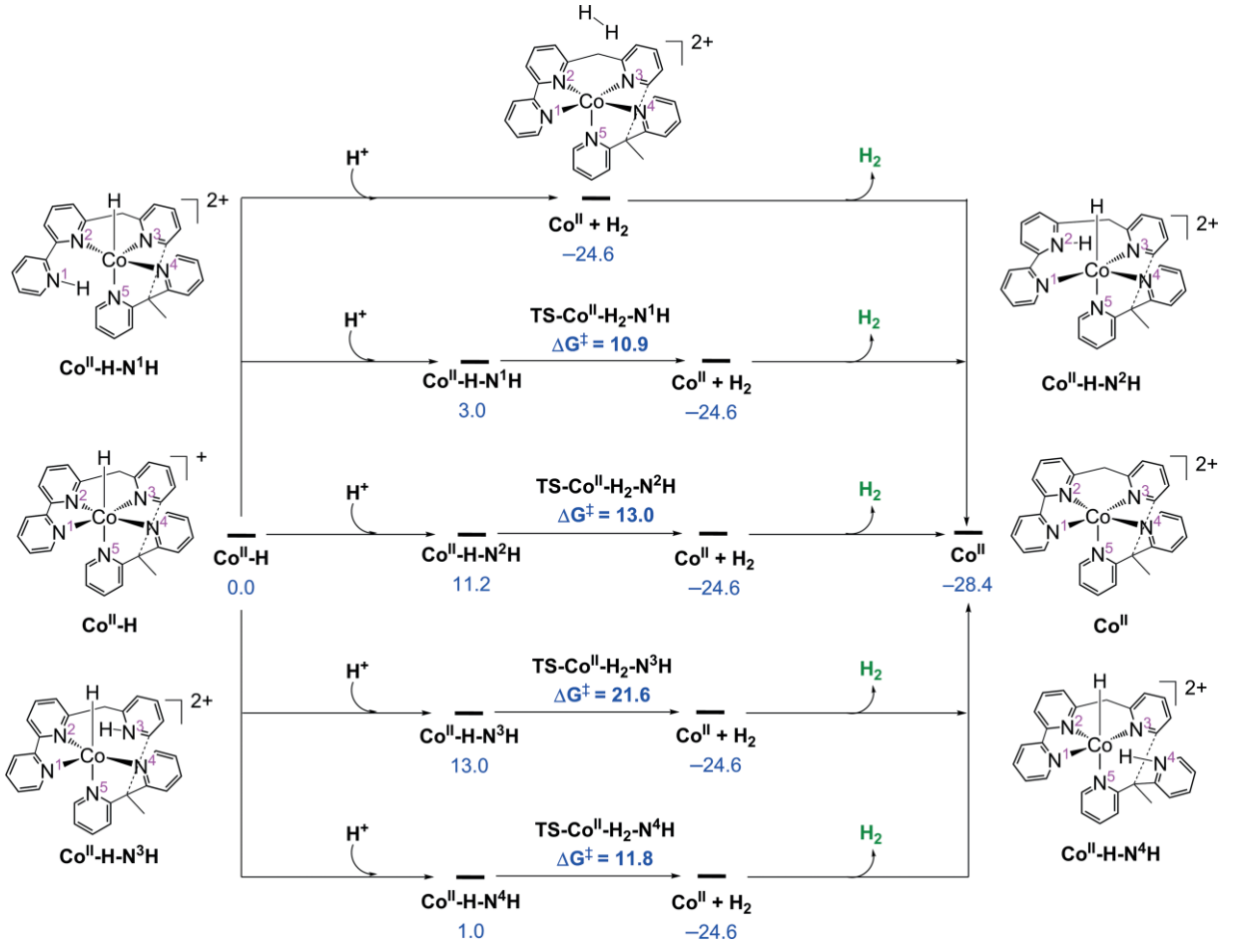

Scheme 4. DFT proposed pathways from the aqueous H_2 generation by heterolytic coupling of protonated Co^{II}–H. Energies are given in kcal/mol. Reprinted from ref.[40e]

olidine) through valence tautomerism was investigated by Verani and co-workers.[53] They confirmed that there is a tautomeric equilibrium between metal-reduced $[Co^{I}(L^{1})]^{-}$ and ligand reduced $[Co^{II}(L^{1\cdot})]^{-}$ species. The metal-reduced $[Co^{I}(L^{1})]^{-}$ could result in the formation Co^{III}–H for catalysis while ligand reduced $[Co^{II}(L^{1\cdot})]^{-}$ would lead to ligand protonation and deactivation of catalyst in the end.

6. Summary and Outlook

There is an urgent need to realize an efficient and low-cost approach for H_2 production to meet our future energy demands and to reduce current dependence on fossil fuels. There has been tremendous progress in developing molecular metal catalysts for HER, especially those based on first-row transition metals. While one class of molecular metal catalysts may be superior to others on certain properties for HER, catalysts that display all the desired properties for future applications are still missing.[12d,12i,54] Considerable efforts have been devoted to the development of novel cobalt catalysts for hydrogen production in aqueous solutions. In comparison to other types of metal complexes, the described Co complexes in this Minireview are generally more soluble and stable for HER in aqueous solutions, and the catalyzed HERs occur in acidic or neutral solutions. The structure-function studies discussed above have provided important insights into the factors controlling the properties of HER. Ligand scaffolds that enable a distorted octahedra geometry, contain redox active, and conjugated moieties have been shown to be favorable for HER by their corresponding Co complexes. The dissociation of one of the coordinating groups from Co center has also been demonstrated during catalytic HER, and such ligand dissociation may be important feature to consider for future ligand design. Efforts to stabilize low valent Co^{I} species under catalysis conditions have shown to be an effective strategy to improve the activity and stability of catalysts, resulting in higher TONs for HER.

Despite the encouraging progress in this field, there still remain significant challenges in discovering cobalt catalysts suitable for future hydrogen production. The reported Co complexes catalyze HER with overpotentials in the range of 420–735 mV, which has to be decreased to be practical for future applications. The tuning of the hydride donor ability of transition-metal hydride may help to develop Co catalysts for HER with low overpotentials.[55] Another major issue is the robustness of Co catalysts under catalytic conditions, strategies to prevent the dissociation of Co ions during catalysis may be the key to improve catalyst stability. The introduction of outer coordina-

tion sphere as the proton relay may enhance the catalytic rates for hydrogen evolution, as has been demonstrated in natural hydrogenases and a number of synthetic catalysts.[38,54b,56] Furthermore, the oxidation of water to oxygen has been studied in a wide range of pHs from acidic to basic solutions. While the reported Co complexes display higher HER activities at acidic or neutral pHs, molecular Co catalysts that are more active at basic solutions may also find applications in the overall water splitting reaction by coupling to water oxidation catalysts that are active at basic pHs.

Acknowledgments

This work is supported by National Science Foundation, CAREER CHE-1352036 to X. Z., CHE-1800201 and OIA-1539035 to C. E. W., and CHE-1531466. We thank the Department of Chemistry at The University of Memphis, and the Department of Chemistry at Mississippi State University.

Keywords: Cobalt · Hydrogen production · Homogeneous catalysis · Pentadentate ligands · Structure-function relationship

[1] N. S. Lewis, D. G. Nocera, *Proc. Natl. Acad. Sci. USA* **2006**, *103*, 15729–15735.
[2] a) B. Li, L. Wang, B. Kang, P. Wang, Y. Qiu, *Sol. Energy Mater. Sol. Cells* **2006**, *90*, 549–573; b) M. A. Green, *J. Mater. Sci. Mater. Electron.* **2007**, *18*, 15–19; c) F. C. Krebs, *Sol. Energy Mater. Sol. Cells* **2009**, *93*, 394–412; d) M. Wright, A. Uddin, *Sol. Energy Mater. Sol. Cells* **2012**, *107*, 87–111.
[3] a) R. E. Blankenship, *Molecular mechanisms of photosynthesis*, John Wiley & Sons, **2014**; b) P. G. Falkowski, J. A. Raven, *Aquatic photosynthesis*, Princeton University Press, **2013**; c) M. F. Hohmann-Marriott, R. E. Blankenship, *Annu. Rev. Plant Biol.* **2011**, *62*, 515–548; d) S. Berardi, S. Drouet, L. Francas, C. Gimbert-Suriñach, M. Guttentag, C. Richmond, T. Stoll, A. Llobet, *Chem. Soc. Rev.* **2014**, *43*, 7501–7519.
[4] a) D. J. Evans, C. J. Pickett, *Chem. Soc. Rev.* **2003**, *32*, 268–275; b) P. M. Vignais, B. Billoud, *Chem. Rev.* **2007**, *107*, 4206–4272; c) C. Tard, C. J. Pickett, *Chem. Rev.* **2009**, *109*, 2245–2274.
[5] a) M. Winkler, J. Esselborn, T. Happe, *Biogenergetics* **2013**, *1827*, 974–985; b) S. S. Nurttila, R. Zaffaroni, S. Mathew, J. N. Reek, *Chem. Commun.* **2019**, *55*, 3081–3084.
[6] a) T. R. Simmons, G. Berggren, M. Bacchi, M. Fontecave, V. Artero, *Coord. Chem. Rev.* **2014**, *270*, 127–150; b) F. Wittkamp, M. Senger, S. Stripp, U.-P. Apfel, *Chem. Commun.* **2018**, *54*, 5934–5942.
[7] A. Silakov, M. T. Olsen, S. Sproules, E. J. Reijerse, T. B. Rauchfuss, W. Lubitz, *Inorg. Chem.* **2012**, *51*, 8617–8628.
[8] Y. Nicolet, A. L. de Lacey, X. Vernède, V. M. Fernandez, E. C. Hatchikian, J. C. Fontecilla-Camps, *J. Am. Chem. Soc.* **2001**, *123*, 1596–1601.
[9] D. Schilter, J. M. Camara, M. T. Huynh, S. Hammes-Schiffer, T. B. Rauchfuss, *Chem. Rev.* **2016**, *116*, 8693–8749.
[10] A. Adamska, A. Silakov, C. Lambertz, O. Rüdiger, T. Happe, E. Reijerse, W. Lubitz, *Angew. Chem. Int. Ed.* **2012**, *51*, 11458–11462; *Angew. Chem.* **2012**, *124*, 11624.
[11] W. Roseboom, A. L. De Lacey, V. M. Fernandez, E. C. Hatchikian, S. P. Albracht, *J. Biol. Inorg. Chem.* **2006**, *11*, 102–118.
[12] a) I. P. Georgakaki, L. M. Thomson, E. J. Lyon, M. B. Hall, M. Y. Darensbourg, *Coord. Chem. Rev.* **2003**, *238*, 255–266; b) T. Liu, M. Y. Darensbourg, *J. Am. Chem. Soc.* **2007**, *129*, 7008–7009; c) M. Wang, Y. Na, M. Gorlov, L. Sun, *Dalton Trans.* **2009**, 6458–6467; d) P. Du, R. Eisenberg, *Energy Environ. Sci.* **2012**, *5*, 6012–6021; e) W. T. Eckenhoff, R. Eisenberg, *Dalton Trans.* **2012**, *41*, 13004–13021; f) M. Wang, L. Chen, L. Sun, *Energy Environ. Sci.* **2012**, *5*, 6763–6778; g) V. S. Thoi, Y. Sun, J. R. Long, C. J. Chang, *Chem. Soc. Rev.* **2013**, *42*, 2388–2400; h) D. Z. Zee, T. Chantarojsiri, J. R. Long, C. J. Chang, *Acc. Chem. Res.* **2015**, *48*, 2027–2036; i) L. Tong, L. Duan, A. Zhou, R. P. Thummel, *Coord. Chem. Rev.* **2020**, *402*, 213079; j) W. T. Eckenhoff, *Coord. Chem. Rev.* **2018**, *373*, 295–316.
[13] a) J. D. Xiao, Q. Shang, Y. Xiong, Q. Zhang, Y. Luo, S. H. Yu, H. L. Jiang, *Angew. Chem. Int. Ed.* **2016**, *55*, 9389–9393; *Angew. Chem.* **2016**, *128*, 9535; b) J. He, J. Wang, Y. Chen, J. Zhang, D. Duan, Y. Wang, Z. Yan, *Chem. Commun.* **2014**, *50*, 7063–7066; c) T. Zhou, Y. Du, A. Borgna, J. Hong, Y. Wang, J. Han, W. Zhang, R. Xu, *Energy Environ. Sci.* **2013**, *6*, 3229–3234; d) S. Pullen, H. Fei, A. Orthaber, S. M. Cohen, S. Ott, *J. Am. Chem. Soc.* **2013**, *135*, 16997–17003; e) X. Zhao, J. Feng, J. Liu, W. Shi, G. Yang, G. C. Wang, P. Cheng, *Angew. Chem. Int. Ed.* **2018**, *57*, 9790–9794; *Angew. Chem.* **2018**, *130*, 9938–9942; f) X. Zhao, J. Feng, J. Liu, J. Lu, W. Shi, G. Yang, G. Wang, P. Feng, P. Cheng, *Adv. Sci.* **2018**, *5*, 1700590.
[14] a) E. J. Popczun, C. G. Read, C. W. Roske, N. S. Lewis, R. E. Schaak, *Angew. Chem. Int. Ed.* **2014**, *53*, 5427–5430; *Angew. Chem.* **2014**, *126*, 5531; b) J. Huang, K. L. Mulfort, P. Du, L. X. Chen, *J. Am. Chem. Soc.* **2012**, *134*, 16472–16475; c) X. Chen, C. Li, M. Grätzel, R. Kostecki, S. S. Mao, *Chem. Soc. Rev.* **2012**, *41*, 7909–7937.
[15] V. Artero, M. Chavarot-Kerlidou, M. Fontecave, *Angew. Chem. Int. Ed.* **2011**, *50*, 7238–7266; *Angew. Chem.* **2011**, *123*, 7376.
[16] a) S. Losse, J. G. Vos, S. Rau, *Coord. Chem. Rev.* **2010**, *254*, 2492–2504; b) W. T. Eckenhoff, W. R. McNamara, P. Du, R. Eisenberg, *Biogenergetics* **2013**, *1827*, 958–973; c) N. Queyriaux, R. T. Jane, J. Massin, V. Artero, M. Chavarot-Kerlidou, *Coord. Chem. Rev.* **2015**, *304*, 3–19; d) X. Zhao, P. Wang, M. Long, *Comments Inorg. Chem.* **2017**, *37*, 238–270; e) J. Huo, Y.-B. Zhang, W.-Y. Zou, X. Hu, Q. Deng, D. Chen, *Catal. Sci. Technol.* **2019**, *9*, 2716–2727; f) D. Dolui, S. Ghorai, A. Dutta, *Coord. Chem. Rev.* **2020**, *416*, 213335.
[17] V. Fourmond, P.-A. Jacques, M. Fontecave, V. Artero, *Inorg. Chem.* **2010**, *49*, 10338–10347.
[18] J. I. Goldsmith, W. R. Hudson, M. S. Lowry, T. H. Anderson, S. Bernhard, *J. Am. Chem. Soc.* **2005**, *127*, 7502–7510.
[19] a) Z. Han, F. Qiu, R. Eisenberg, P. L. Holland, T. D. Krauss, *Science* **2012**, *338*, 1321–1324; b) Z. Han, R. Eisenberg, *Acc. Chem. Res.* **2014**, *47*, 2537–2544; c) Z.-J. Li, X.-B. Li, J.-J. Wang, S. Yu, C.-B. Li, C.-H. Tung, L.-Z. Wu, *Energy Environ. Sci.* **2013**, *6*, 465–469.
[20] Y. Sun, J. Sun, J. R. Long, P. Yang, C. J. Chang, *Chem. Sci.* **2013**, *4*, 118–124.
[21] R. Gueret, L. Poulard, M. Oshinowo, J. Chauvin, M. Dahmane, G. Dupeyre, P. P. Lainé, J. Fortage, M.-N. l. Collomb, *ACS Catal.* **2018**, *8*, 3792–3802.
[22] Y. Sun, J. P. Bigi, N. A. Piro, M. L. Tang, J. R. Long, C. J. Chang, *J. Am. Chem. Soc.* **2011**, *133*, 9212–9215.
[23] M. Nippe, R. S. Khnayzer, J. A. Panetier, D. Z. Zee, B. S. Olaiya, M. Head-Gordon, C. J. Chang, F. N. Castellano, J. R. Long, *Chem. Sci.* **2013**, *4*, 3934–3945.
[24] a) J. W. Jurss, R. S. Khnayzer, J. A. Panetier, K. A. El Roz, E. M. Nichols, M. Head-Gordon, J. R. Long, F. N. Castellano, C. J. Chang, *Chem. Sci.* **2015**, *6*, 4954–4972; b) L. Chen, A. Khadivi, M. Singh, J. W. Jurss, *Inorg. Chem. Front.* **2017**, *4*, 1649–1653.
[25] a) J. P. Bigi, T. E. Hanna, W. H. Harman, A. Chang, C. J. Chang, *Chem. Commun.* **2010**, *46*, 958–960; b) R. Khnayzer, V. Thoi, M. Nippe, A. King, J. Jurss, K. El Roz, J. Long, C. Chang, F. Castellano, *Energy Environ. Sci.* **2014**, *7*, 1477–1488.
[26] C. Bachmann, M. Guttentag, B. Spingler, R. Alberto, *Inorg. Chem.* **2013**, *52*, 6055–6061.
[27] E. Deponti, A. Luisa, M. Natali, E. Iengo, F. Scandola, *Dalton Trans.* **2014**, *43*, 16345–16353.
[28] M. Wilken, I. Siewert, *ChemElectroChem* **2020**, *7*, 217–221.
[29] J. Xie, Q. Zhou, C. Li, W. Wang, Y. Hou, B. Zhang, X. Wang, *Chem. Commun.* **2014**, *50*, 6520–6522.
[30] W. K. Lo, C. E. Castillo, R. Gueret, J. r. m. Fortage, M. Rebarz, M. Sliwa, F. Thomas, C. J. McAdam, G. B. Jameson, D. A. McMorran, J. D. Crowley, M.-N. Collomb, A. G. Blackman, *Inorg. Chem.* **2016**, *55*, 4564–4581.
[31] P. Zhang, M. Wang, F. Gloaguen, L. Chen, F. Quentel, L. Sun, *Chem. Commun.* **2013**, *49*, 9455–9457.
[32] D. Basu, S. Mazumder, X. Shi, H. Baydoun, J. Niklas, O. Poluektov, H. B. Schlegel, C. N. Verani, *Angew. Chem. Int. Ed.* **2015**, *54*, 2105–2110; *Angew. Chem.* **2015**, *127*, 2133.
[33] D. Basu, S. Mazumder, X. Shi, R. J. Staples, H. B. Schlegel, C. N. Verani, *Angew. Chem. Int. Ed.* **2015**, *54*, 7139–7143; *Angew. Chem.* **2015**, *127*, 7245.

[34] D. Basu, S. Mazumder, K. K. Kpogo, C. N. Verani, *Dalton Trans.* **2019**, *48*, 14669–14677.
[35] a) X. Song, H. Wen, C. Ma, H. Chen, C. Chen, *New J. Chem.* **2015**, *39*, 1734–1741; b) X.-W. Song, Y. Meng, C.-L. Zhang, C.-B. Ma, C.-N. Chen, *Inorg. Chem. Commun.* **2017**, *76*, 52–54.
[36] A. Call, Z. Codolà, F. Acuña-Parés, J. Lloret-Fillol, *Chem. Eur. J.* **2014**, *20*, 6171–6183.
[37] J. W. Wang, K. Yamauchi, H. H. Huang, J. K. Sun, Z. M. Luo, D. C. Zhong, T. B. Lu, K. Sakai, *Angew. Chem. Int. Ed.* **2019**, *58*, 10923–10927; *Angew. Chem.* **2019**, *131*, 260.
[38] R. Gueret, C. E. Castillo, M. Rebarz, F. Thomas, M. Sliwa, J. Chauvin, B. Dautreppe, J. Pécaut, J. Fortage, M.-N. Collomb, *Inorg. Chem.* **2019**, *58*, 9043–9056.
[39] C. Bachmann, B. Probst, M. Guttentag, R. Alberto, *Chem. Commun.* **2014**, *50*, 6737–6739.
[40] a) W. M. Singh, T. Baine, S. Kudo, S. Tian, X. A. Ma, H. Zhou, N. J. DeYonker, T. C. Pham, J. C. Bollinger, D. L. Baker, B. Yan, C. E. Webster, X. Zhao, *Angew. Chem. Int. Ed.* **2012**, *51*, 5941–5944; *Angew. Chem.* **2012**, *124*, 6043; b) M. Vennampalli, G. Liang, L. Katta, C. E. Webster, X. Zhao, *Inorg. Chem.* **2014**, *53*, 10094–10100; c) P. Wang, G. Liang, M. R. Reddy, M. Long, K. Driskill, C. Lyons, B. Donnadieu, J. C. Bollinger, C. E. Webster, X. Zhao, *J. Am. Chem. Soc.* **2018**, *140*, 9219–9229; d) P. Wang, G. Liang, C. L. Boyd, C. E. Webster, X. Zhao, *Eur. J. Inorg. Chem.* **2019**, *2019*, 2134–2139; e) P. Wang, G. Liang, N. Smith, K. Hill, B. Donnadieu, C. E. Webster, X. Zhao, *Angew. Chem. Int. Ed.* **2020**, *59*, 12694–12697; f) B. Shan, T. Baine, X. A. N. Ma, X. Zhao, R. H. Schmehl, *Inorg. Chem.* **2013**, *52*, 4853–4859; g) A. Lewandowska-Andralojc, T. Baine, X. Zhao, J. T. Muckerman, E. Fujita, D. E. Polyansky, *Inorg. Chem.* **2015**, *54*, 4310–4321.
[41] B. Radaram, J. A. Ivie, W. M. Singh, R. M. Grudzien, J. H. Reibenspies, C. E. Webster, X. Zhao, *Inorg. Chem.* **2011**, *50*, 10564–10571.
[42] Z.-J. Li, F. Zhan, H. Xiao, X. Zhang, Q.-Y. Kong, X.-B. Fan, W.-Q. Liu, M.-Y. Huang, C. Huang, Y.-J. Gao, X.-B. Li, Q.-Y. Meng, K. Feng, B. Chen, C.-H. Tung, H.-F. Zhao, Y. Tao, L.-Z. Wu, *J. Phys. Chem. Lett.* **2016**, *7*, 5253–5258.
[43] a) B. H. Solis, S. Hammes-Schiffer, *Inorg. Chem.* **2011**, *50*, 11252–11262; b) B. H. Solis, S. Hammes-Schiffer, *J. Am. Chem. Soc.* **2011**, *133*, 19036–19039; c) U. Koelle, S. Paul, *Inorg. Chem.* **1986**, *25*, 2689–2694.
[44] N. Queyriaux, D. Sun, J. Fize, J. Pécaut, M. J. Field, M. Chavarot-Kerlidou, V. Artero, *J. Am. Chem. Soc.* **2019**, *142*, 274–282.
[45] a) X. Hu, B. S. Brunschwig, J. C. Peters, *J. Am. Chem. Soc.* **2007**, *129*, 8988–8998; b) S. C. Marinescu, J. R. Winkler, H. B. Gray, *Proc. Natl. Acad. Sci. USA* **2012**, *109*, 15127–15131; c) W. M. Singh, M. Mirmohades, R. T. Jane, T. A. White, L. Hammarstrom, A. Thapper, R. Lomoth, S. Ott, *Chem. Commun.* **2013**, *49*, 8638–8640; d) J. Schneider, H. Jia, J. T. Muckerman, E. Fujita, *Chem. Soc. Rev.* **2012**, *41*, 2036–2051.
[46] M. Fang, E. S. Wiedner, W. G. Dougherty, W. S. Kassel, T. Liu, D. L. DuBois, R. M. Bullock, *Organometallics* **2014**, *33*, 5820–5833.
[47] D. C. Grills, D. E. Polyansky, E. Fujita, *ChemSusChem* **2017**, *10*, 4359–4373.
[48] S. Grau, M. Schilling, D. Moonshiram, J. Benet-Buchholz, S. Luber, A. Llobet, C. Gimbert-Suriñach, *ChemSusChem* **2020**, *13*, 2745–2752.
[49] A. E. King, Y. Surendranath, N. A. Piro, J. P. Bigi, J. R. Long, C. J. Chang, *Chem. Sci.* **2013**, *4*, 1578–1587.
[50] L. Kohler, J. Niklas, R. C. Johnson, M. Zeller, O. G. Poluektov, K. L. Mulfort, *Inorg. Chem.* **2018**, *57*, 1697–1709.
[51] G. Smolentsev, M. A. Soldatov, B. Probst, C. Bachmann, N. Azzaroli, R. Alberto, M. Nachtegaal, J. A. van Bokhoven, *ChemSusChem* **2018**, *11*, 3087–3091.
[52] R. H. Crabtree, *Chem. Rev.* **2015**, *115*, 127–150.
[53] H. Baydoun, S. Mazumder, H. B. Schlegel, C. N. Verani, *Chem. Eur. J.* **2017**, *23*, 9266–9271.
[54] a) J.-W. Wang, W.-J. Liu, D.-C. Zhong, T.-B. Lu, *Coord. Chem. Rev.* **2019**, *378*, 237–261; b) M. L. Helm, M. P. Stewart, R. M. Bullock, M. R. DuBois, D. L. DuBois, *Science* **2011**, *333*, 863–866.
[55] A. L. Ostericher, K. M. Waldie, C. P. Kubiak, *ACS Catal.* **2018**, *8*, 9596–9603.
[56] a) R. M. Bullock, M. L. Helm, *Acc. Chem. Res.* **2015**, *48*, 2017–2026; b) D. L. DuBois, *Inorg. Chem.* **2014**, *53*, 3935–3960; c) R. M. Bullock, A. M. Appel, M. L. Helm, *Chem. Commun.* **2014**, *50*, 3125–3143; d) G. M. Jacobsen, J. Y. Yang, B. Twamley, A. D. Wilson, R. M. Bullock, M. R. DuBois, D. L. DuBois, *Energy Environ. Sci.* **2008**, *1*, 167–174.

Received: June 15, 2020